



## Identification of nonlinear anti-vibration isolator properties

Fares Mezghani<sup>a,b</sup>, Alfonso Fernández Del Rincón<sup>b</sup>, Mohamed Amine Ben Souf<sup>a</sup>, Pablo García Fernández<sup>b</sup>, Fakher Chaari<sup>a,\*</sup>, Fernando Viadero Rueda<sup>b</sup>, Mohamed Haddar<sup>a</sup>

<sup>a</sup> Laboratory of Mechanics, Modelling and Production, National School of Engineering of Sfax, University of Sfax, Sfax, Tunisia

<sup>b</sup> Laboratory of Structural and Mechanical Engineering, Superior Technical School of Industrial Engineering and Telecommunications, University of Cantabria, Santander, Spain

### ARTICLE INFO

#### Article history:

Received 25 December 2016

Accepted 13 March 2017

Available online 2 April 2017

#### Keywords:

Anti-vibration isolator

Dynamic behaviour

Transmissibility measured data

Numerical simulations

### ABSTRACT

Vibrations are classified among the major problems for engineering structures. Anti-vibration isolators are used to absorb vibration energy and minimise transmitted force which can cause damage. The isolator is modelled as a parallel combination of stiffness and damping elements. The main purpose of the model is to enable designers to predict the dynamic response of systems under different structural excitations and boundary conditions. A nonlinear identification method, discussed in this paper, aims to provide a tool for engineers to extract information about the nonlinear dynamic behaviour using measured data from experiments. The proposed method is demonstrated and validated with numerical simulations. Thus, this technique is applied to determine the nonlinear parameters of a commercial metal mesh isolator. Nonlinear stiffness and nonlinear damping can decrease with the increase in the amplitude of the base excitation. The softening behaviour of the mesh isolator is clearly visible.

© 2017 Académie des sciences. Published by Elsevier Masson SAS. All rights reserved.

## 1. Introduction

In many engineering applications, it is required to minimise the transfer of vibrations from the source to the receiver. In order to solve this problem and reduce the transmitted vibration, a vibration isolator should be added. From several isolation techniques, the passive isolator has been widely applied in engineering due to its simple design and high reliability. Different kinds of passive isolators are applied in many fields. For instance, typical vibration isolators employ metal coil spring to store the energy due to resilience and to maintain the force between contacting surfaces. Elastomeric shock mounts, such as rubber isolators that absorb mechanical energy by deforming, play an important role in noise and vibration control. They are widely used in automotive engines [1], aircraft components, industrial machinery, and building foundations. In practice, air spring, pneumatic and elastomeric vibration mount, are also commonly used as an important fundamental part of mechanical equipment requiring low natural frequency isolation and automobile suspension system [2]. Viscoelastic material isolators are considered as a relatively new damping material and have been extensively used in aerospace applications [3]. There are various types of this kind [4–6], such as the vibration isolator using solid and liquid mixtures (SALiM) [7], which was inspired by Yamamoto [8]. Further to that, Courtney carried out some experiments on a shock-absorbing liquid

\* Corresponding author.

E-mail address: fakher.chaari@gmail.com (F. Chaari).

absorber to validate its basic properties, and referred to as the SALiM liquid [9,10]. Another kind of passive isolator is the passive negative stiffness isolator [11,12], which is a revolutionary concept in low-frequency vibration isolation. This isolator is provided by a spring that supports a load, combined with two springs, which are called corrector or auxiliary springs, acting as a negative stiffness mechanism. The metal mesh isolator, which is essentially comprised of stainless steel wires crimped, rolled or compressed into any geometric shape that is required, is one of the important passive vibration isolation products stop-shock. It can provide a solution for many engineering applications, for example, engines and gearboxes supports, railway lines and suspension bump stops. It has not only higher stiffness than the elastomeric materials, but also offers larger hysteresis loops and provides excellent isolation performance [13].

In order to design a nonlinear system and predict the dynamic behaviour, the modal analysis method, based on mathematical models of a single-degree-of-freedom system, is used. The modal quantities depend on several variables: amplitude of vibration, frequency of excitation, stiffness, and damping parameters. The main purpose to use nonlinear modal analysis methods is to allow engineers to identify and quantify the nonlinearity in a standard testing environment. The most significant application of modal testing is to compare the numerical analysis with experimental data and to apply the necessary changes on the model, in order to obtain satisfactory results.

The identification and quantification of nonlinearity has drawn much attention. There are many techniques currently available, presented in [14,15]. Worden and Tomlinson [16] summarised the background of harmonic balance method and the Hilbert transform. The latter was used by Feldman to propose a method that allows one to study the dynamic system for: free vibration analysis “FREEVIB” [17] and forced vibration analysis “FORCEVIB” [18]. Kerschen et al. [19] classified the identification methods according to seven categories. Some cited methods are: the restoring force surface (RFS) [20], the inverse method [21] and the linearity plots [22]. The RFS works in the time domain and the starting point is the application of Newton’s second law. Moreover, Rice [23] identified the nonlinear parameters using equivalent linearisation and determined the optimum one by minimising the average of the least square of the error. Guo [24] evaluated the transmissibility of a nonlinear viscously damped vibration system under harmonic excitation using a new method, based on the Ritz–Galerkin method, to investigate the effect of the damping characterisation parameters on this system. A. Carrella [25–27] has recently presented a new approach, COde for Nonlinear Characterisation from mEasured Response To vibratiOn, to identify and quantify the dynamic behaviour of vibration isolators, based on the analysis of experimental data. CONCERTO is applied to a single degree of freedom (SDOF) system which is subjected to harmonic base excitation or harmonic force excitation. The principle, upon which the approach is based, is effectively a linearisation; at a given response amplitude, the stiffness and the damping are considered constant. It is also assumed that the system responds at the same frequency as the excitation.

The main novelty of this work is the employment of the identification method mentioned previously to reconstruct the nonlinear stiffness and damping functions of a metal mesh isolator. This paper aims at investigating the dynamic properties of the examined isolator under different levels of excitation in order to improve the reduction of the transmitted vibrations. This paper is organised as follows: the following section introduces the procedure proposed in this work; in the third section, a comparison is performed with an existing nonlinear identification method based on the measured transmissibility [27] in order to validate the numerical model qualitatively and quantitatively; the transmissibility measured data are analysed to characterise and identify the nonlinear stiffness and damping of the investigated isolator in the fourth section.

## 2. Theoretical study

In this section, the used methodology is presented and discussed. It consists of the measurement of the transmissibility (displacement) from appropriate responses, on the one hand and on the extracting frequency (stiffness) and damping functions, on the other hand.

### 2.1. Overview of CONCERTO: Code for Nonlinear Characterisation from mEasured Response To vibratiOn

CONCERTO, presented in [25–27], is a frequency-domain method, whose aim is the identification and quantification of nonlinear parameters [25] from measured FRF [26] and transmissibility data [27]. This method is used to analyse numerical and experimental data [27].

The proposed SDOF (see Fig. 1) identification method, based on the assumption that the studied system with nonlinear stiffness and damping subjected to harmonic base excitation, can be depicted through the equation of motion as follows:

$$m\ddot{z} + k(1 + j\eta)z = m\omega^2 Y \sin(\omega t) \quad (1)$$

where  $z = x - y$  represents the deformation of the mount,  $\omega$  the excitation frequency,  $k$  and  $\eta$  are the stiffness and damping loss factor respectively.

The absolute transmissibility is defined as the non-dimensional quantity that tells how the motion is transmitted from the base to the mass at various frequencies. It is measured as the ratio between the output and the input displacements.

$$|T| = \left| \frac{X}{Y} \right| = \left| \frac{k(1 + j\eta)}{k(1 + j\eta) - m\omega^2} \right| \quad (2)$$

This can be rewritten in terms of modal quantities as:

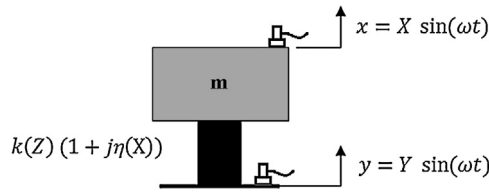


Fig. 1. Model of SDOF system with a nonlinear isolator under a base excitation.

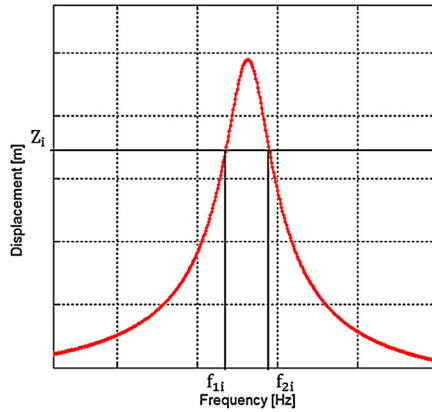


Fig. 2. Linearisation process of CONCERTO.

$$|T| = \left| \frac{X}{Y} \right| = \left| \frac{\omega_0^2 + j\omega_0^2\eta}{\omega_0^2 - \omega^2 + j\omega_0^2\eta} \right| \tag{3}$$

For a given amplitude  $Z_i$ , there is a pair of frequencies points (see Fig. 2). The displacement-vs.-frequency curve contains information that is required to calculate the natural frequency  $\omega_0(Z_i)$  and the loss factor  $\eta(Z_i)$  at that particular amplitude as:

$$\omega_0^2(Z_i) = \frac{(R_{2i} - R_{1i})(R_{2i}\omega_{2i}^2 - R_{1i}\omega_{1i}^2) + (I_{2i} - I_{1i})(I_{2i}\omega_{2i}^2 - I_{1i}\omega_{1i}^2)}{(R_{2i} - R_{1i})^2 + (I_{2i} - I_{1i})^2} \tag{4}$$

$$\eta(Z_i) = \left| \frac{-(I_{2i} - I_{1i})(R_{2i}\omega_{2i}^2 - R_{1i}\omega_{1i}^2) + (R_{2i} - R_{1i})(I_{2i}\omega_{2i}^2 - I_{1i}\omega_{1i}^2)}{\omega_0^2(Z_i)((R_{2i} - R_{1i})^2 + (I_{2i} - I_{1i})^2)} \right| \tag{5}$$

where  $R_1$  and  $R_2$  ( $I_1$  and  $I_2$ ) are the real (imaginary) parts of the transmissibility at the amplitude  $Z_i$ , which have been measured at frequencies  $\omega_1$  and  $\omega_2$ , before and after the resonance peak, respectively.

In order to quantify nonlinear parameters, it is necessary to evaluate the stiffness and damping functions, from natural frequency and loss factor expressions.

Once the model mass, presenting the mass of the system divided by the number of mounts in the system, has been determined, the stiffness function  $k(Z_i)$  can thus be obtained by multiplying the mass by the natural frequency expressed in Eq. (4).

$$k(Z_i) = \omega_0^2(Z_i)m \tag{6}$$

In addition, the damping function  $C(Z_i)$  can be extracted using the relationship [25]:

$$C(Z_i) = \eta(Z_i)\omega_0(Z_i)m \tag{7}$$

2.2. Analytical stiffness and damping functions using Harmonic Balance

In order to evaluate the efficiency of the method, analytical expressions for stiffness and damping functions have been derived using the Harmonic Balance Method to solve nonlinear differential equations [16].

In fact, the effective expressions correspond to the stiffness and damping of a linearised system under the assumption that the latter responds at the same frequency as the harmonic excitation [26]. This is equivalent to the analytical expressions determined by applying the first-order expansion of the harmonic balance approximation in the steady state. According to experimental investigations, this basic assumption is reasonable and valid. Otherwise, it is proved that the nonlinear parameters dependence is dominated by the vibration amplitude [28].

The dynamic equation describing the motion of a SDOF system, subjected to a harmonic excitation, could be written as:

$$m\ddot{z} + f_d(\dot{z}) + f_s(z) = y(t) \tag{8}$$

where  $z$  and  $y$  denote the response and the excitation, respectively.  $f_d(\dot{z})$  is the nonlinear damping function, and  $f_s(z)$  is the nonlinear stiffness function.

For stable state harmonic vibration, the displacement response can be expressed as:

$$z(t) = Z \sin(\omega t) \tag{9}$$

The analysis will be simplified by considering the equation of motion as follows:

$$m\ddot{z} + C_q\dot{z} + K_qz = y(t) \tag{10}$$

where  $C_q$  and  $K_q$  present the equivalent damping and stiffness, respectively.

2.2.1. Nonlinear stiffness

The nonlinear stiffness function can be expanded using the Fourier series, neglecting all the higher-order terms and considering only the fundamental term (first harmonic).

So:

$$f_s(z) \cong a_{k0} + a_{k1} \cos(\omega t) + b_{k1} \sin(\omega t) = K_qz(t) \tag{11}$$

where  $a_{k0}$ ,  $a_{k1}$  and  $b_{k1}$  are the Fourier coefficients of the fundamental term expressed as:

$$a_{k0} = \frac{1}{2\pi} \int_0^{2\pi} f_s(z(t)) d\theta$$

$$a_{k1} = \frac{1}{\pi} \int_0^{2\pi} f_s(z(t)) \cos \theta d\theta$$

$$b_{k1} = \frac{1}{\pi} \int_0^{2\pi} f_s(z(t)) \sin \theta d\theta \tag{12}$$

The mathematical model of a cubic stiffness element can be expressed as:

$$f_s(z) = kz + k_{nl}z^3 \tag{13}$$

So, substituting Eq. (13) into Eq. (12), the Fourier coefficients will be calculated:

$$a_{k0} = 0$$

$$a_{k1} = 0$$

$$b_{k1} = k_1Z + \frac{3}{4}k_{nl}Z \tag{14}$$

Therefore,

$$K_q = k + \frac{3}{4}k_{nl}Z^2 \tag{15}$$

where  $k$  and  $k_{nl}$  represent the linear and the nonlinear stiffness parameters, respectively.

2.2.2. Nonlinear damping

The nonlinear damping function can be rewritten as follows:

$$f_d(\dot{z}(t)) \cong a_{c0} + a_{c1} \cos(\omega t) + b_{c1} \sin(\omega t) = C_q\dot{z}(t) \tag{16}$$

where  $a_{c0}$ ,  $a_{c1}$  and  $b_{c1}$  are the Fourier coefficient of the fundamental term.

$$a_{c0} = \frac{1}{2\pi} \int_0^{2\pi} f_d(\dot{z}(t)) d\theta$$

$$a_{c1} = \frac{1}{\pi} \int_0^{2\pi} f_d(\dot{z}(t)) \cos \theta d\theta$$

$$b_{c1} = \frac{1}{\pi} \int_0^{2\pi} f_d(\dot{z}(t)) \sin \theta d\theta \tag{17}$$

**Table 1**  
Type and values of nonlinearities for the numerical simulation.

| Mass $m = 1.5$ kg, damping coefficient $c = 0.8$ Ns/m, $k = 6000$ N/m |                                |                    |  |
|---|--------------------------------|--------------------|--|
| Nonlinearity  | Damping $f_c$                  | Stiffness $f_k$    | Values   |
| Cubic stiffness +<br>Quadratic damping                                | $f_c = C_{nl}\dot{z} \dot{z} $ | $f_k = k_{nl} z^2$ | $k_{nl} = 7 \cdot 10^6$ N/m <sup>3</sup><br>$C_{nl} = 8$ Ns <sup>2</sup> /m <sup>2</sup> |

Combining Eq. (16) and Eq. (17) leads to:

$$C_q = \frac{a_{c_1}}{\omega Z} = \frac{1}{\omega Z \pi} \int_0^{2\pi} f_d(\omega Z \cos \theta) \cos \theta \, d\theta \tag{18}$$

The mathematical model of a quadratic damping element can be expressed as:

$$f_d(\dot{z}) = c\dot{z} + c_{nl}\dot{z}|\dot{z}| \tag{19}$$

Then the equivalent damping is given by:

$$C_q = \frac{c}{\omega Z \pi} \int_0^{2\pi} \omega Z \cos \theta \cos \theta \, d\theta + \frac{c_{nl}}{\omega Z \pi} \int_0^{2\pi} \omega Z \cos \theta |\omega Z \cos \theta| \cos \theta \, d\theta \tag{20}$$

After integration, this becomes:

$$C_q = c + \frac{8}{3\pi} c_{nl} \omega Z \tag{21}$$

where  $\omega$  is the natural frequency of linear system and  $Z$  is the amplitude of the response at the steady state.  $c$  and  $c_{nl}$  represent the linear and the nonlinear damping parameters, respectively.

### 3. Numerical simulations of transmissibility data for nonlinear systems

In this section, a set of numerical simulations of nonlinear SDOF systems are presented to illustrate the applicability of the approach discussed above. Table 1 summarises the type of nonlinearity and the numerical values used in each case. In addition, the parameters of the underlying linear system are described in Table 1. All the simulation refer to the systems, which are modelled as:

$$m\ddot{z} + c\dot{z} + f_c(\dot{z}) + kz + f_k(z) = m\omega^2 Y \sin(\omega t) \tag{22}$$

where  $z = x - y$  is the relative displacement between the mass and the base and  $Y$  the amplitude of the base excitation.  $f_c$  and  $f_k$  represent the nonlinear damping and stiffness, respectively.

Eq. (22) has been solved using direct integration with the Matlab solver ODE45, which is the Runge–Kutta 4th- and 5th-order method for ordinary differential equations at different excitation frequencies. Then, the absolute displacement has been determined by computing the ratio between the Fourier coefficient of the response and the amplitude of the base excitation.

In order to validate the results obtained with the CONCERTO approach, a comparison is performed with the nonlinear identification method based on measured transmissibility and presented in [27] and then with the analytical expressions for the stiffness functions explained in section 2.3. Figs. 3–4 show the results obtained in analysing the transmissibility of a system with combined nonlinearities (quadratic damping + cubic stiffness) and excited by a harmonic base oscillation with an amplitude of  $Y = 0.4 \cdot 10^{-3}$  m and  $Y = 0.15 \cdot 10^{-3}$  m, respectively.

The information about the nonlinearities of the system is provided in the two plots: one depicts stiffness, Eq. (15), and the other damping, Eq. (16), as a function of the amplitude of vibration displacement response of the mass.

From the stiffness and damping plots, it can be seen that by increasing the level of excitation, and thus the amplitude of the response, there is an increase in stiffness and damping. This increase suggests a hardening stiffness.

From the Figs. 3(b, c) and 4(b, c), we remark that these results show a quite noticeable agreement between the extracted stiffness and its analytical equivalent expression. But errors are introduced in the estimation of damping due, perhaps, to CONCERTO’s interpolation whose limitations are that the determination of the stiffness and damping values is based on points that physically do not exist but are a pure numerical artefact [26].

### 4. Experimental set up, results and discussions

In the following section, an experimental investigation is performed to determine the nonlinear properties of a commercially metal mesh isolator that can be inserted between the source of vibrations and the receiver. Experimental tests were designed to characterise and to identify the nonlinear stiffness and damping of this isolator.

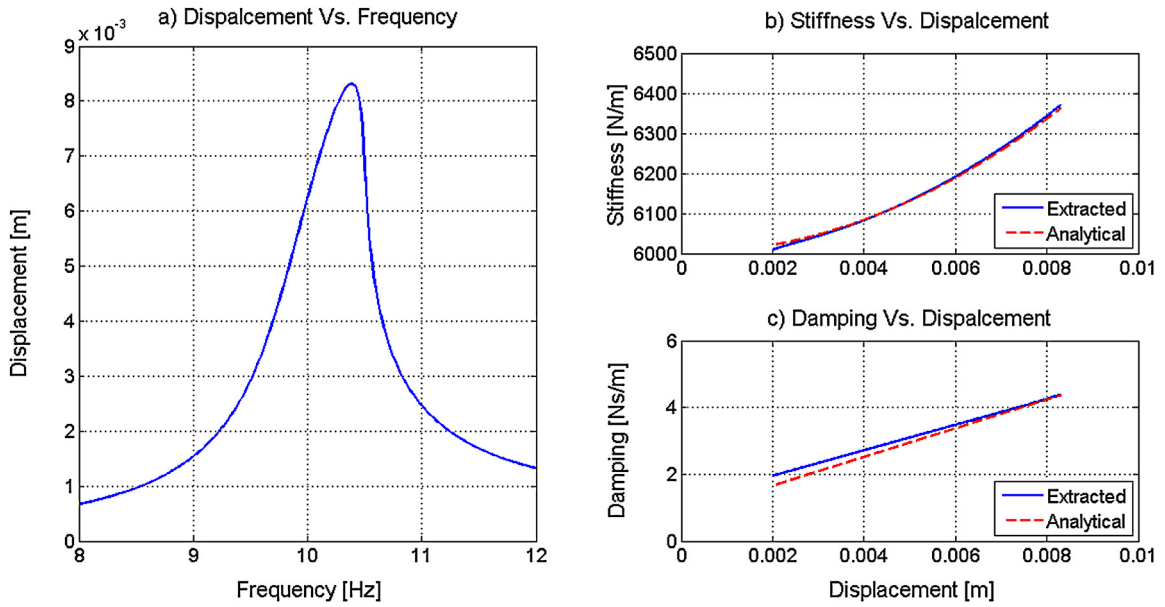


Fig. 3. Numerical analysis of the system with cubic stiffness and quadratic damping at base-displacement level of  $0.4 \cdot 10^{-3}$  m.

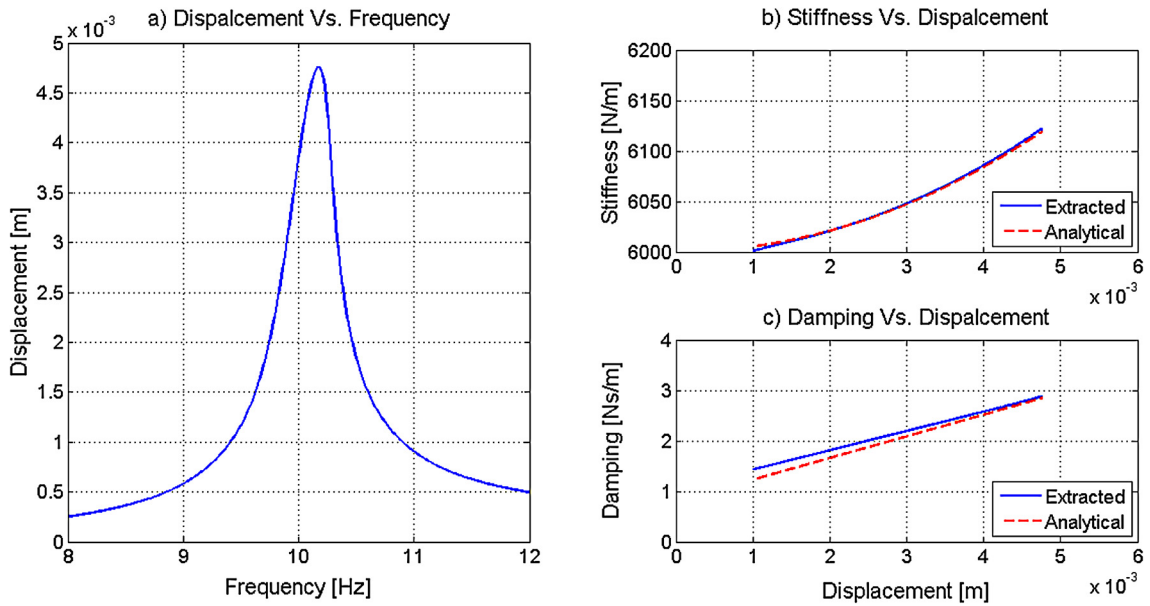


Fig. 4. Numerical analysis of the system with cubic stiffness and quadratic damping at base-displacement level of  $0.15 \cdot 10^{-3}$  m.

#### 4.1. Measurement

The experiments are performed in an electrodynamic shaker Gearing and Watson V400, connected to an amplifier DSA4-8k. The experimental set up is displayed in Fig. 5. The exciter was positioned vertically and was controlled by a USB laser system through the Dactron associated software for data acquisition and analysis. Two accelerometers (Brüel & Kjør, type 4398) are axially placed: one on the shaker table and another on the mass plate. The transmissibility could be determined by the ratio of the two signals.

In order to study the mounts behaviour under different static loads, three masses were used:  $M_1$ ,  $M_2$  and  $M_3$ , which are dependent on the number of plates. The mass values used during the test are given in Table 2.

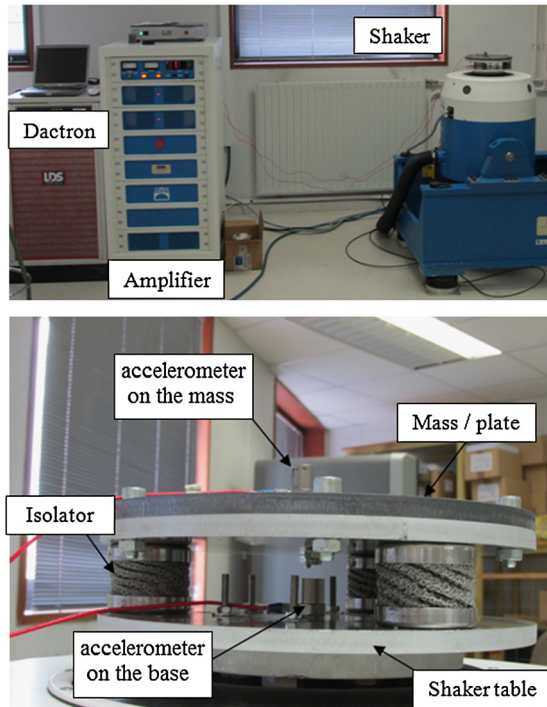


Fig. 5. Test machine.

**Table 2**

Values and number of plates used during the test.

|       | Number of plates | Mass values |
|-------|------------------|-------------|
| $M_1$ | 1                | 5686.2 g    |
| $M_2$ | 4                | 17552.6 g   |
| $M_3$ | 7                | 29270.3 g   |

#### 4.2. Material: the test object

The metal mesh isolators are essentially stainless steel wires, woven using a knitting machine, rolled and/or pressed into the required geometric shape via a press mould. The density of the mesh isolators were determined by the knitting and pressing method. Metal mesh material can be manufactured to accommodate specific application needs including railway, engine mounts, and vibration absorbers.

Five models of isolators (A, B, C, D, E), that differ in their density as shown in Fig. 6, are selected as the test element for the experimental investigation. Measurements, which have been carried out according to the method established above, are aimed at identifying the dynamic characterisation of the nonlinear isolator.

#### 4.3. Sine sweep excitation

Three levels of acceleration ( $a_1 = 1 \text{ m/s}^2$ ,  $a_2 = 2 \text{ m/s}^2$  and  $a_3 = 3 \text{ m/s}^2$ ), for each mass and isolator, have been used for exciting the structure with the stepped-sine signal starting at 5 Hz and increasing with a constant frequency step to a maximum frequency of 50 Hz. At each excited frequency, the transmissibility was detected using the ratio of the vibration amplitude being measured in the system to the vibration amplitude entering the system. Tests were performed for each of the aforementioned cases.

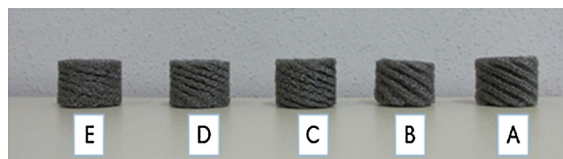


Fig. 6. Five models of isolators.

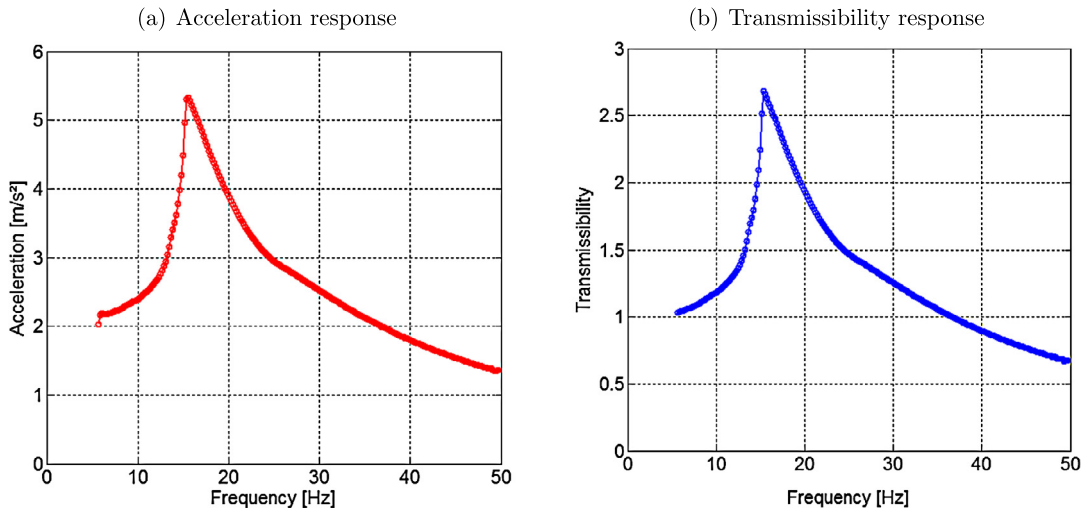


Fig. 7. Sine sweep test; model A, mass 1, acceleration 2 m/s<sup>2</sup>.

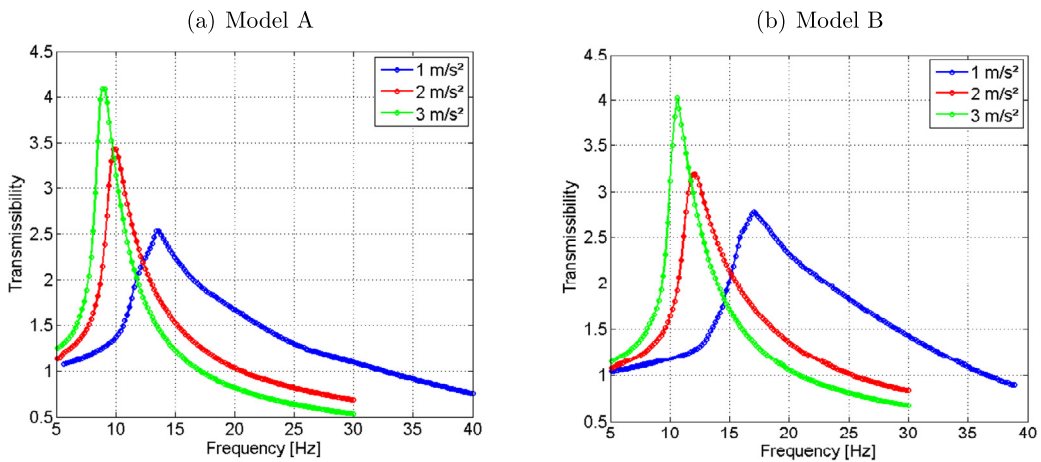


Fig. 8. Sine sweep test; mass 2.

Figs. 7(a, b) present the results of the sine sweep of the isolator model A, obtained with  $M_1$  and excited by the second level of acceleration ( $a_2 = 2 \text{ m/s}^2$ ), which is kept constant during the test. Fig. 7(a) depicts the acceleration response measured by the output accelerometer of the mass. Fig. 7(b) shows the transmissibility, which was computed as the ratio of the mass acceleration measured by the accelerometer on the mass, and the base acceleration measured by the accelerometer on the base, as indicated in Fig. 5.

It is observed that the peak on the curve, at around 15 Hz, is representative of that isolator’s resonance frequency. It can be also noticed that the vibration isolation occurs when the curve crosses the transmissibility-axis into one, i.e. for frequencies above 36.5 Hz.

Fig. 8(a, b) show the results of the transmissibility response of the isolators A and B using  $M_2$  and for the three level of acceleration inputs. From Figs. 8(a) and 8(b), it can be seen that by increasing the level of the acceleration, the resonance frequency of the system decreases and the amplitude increases; similarly, the transmissibility decreases at high frequencies.

Otherwise, the higher the level of excitation, the lower is the damping and the stiffness of the isolator, and the earlier is the vibration isolation region. The deviation, lean of the curve towards lower frequencies, is a result of the softening behaviour.

The curves of transmissibility of the both isolators B and C measured for the second level of acceleration ( $a_2 = 2 \text{ m/s}^2$ ) and using the three masses ( $M_1, M_2$  and  $M_3$ ) are shown in Figs. 9(a, b). It is noteworthy that, as the weight of the preload increases, the resonance frequency of the system decreases and the frequency, at which the transmissibility is less than one, decreases, from 43 Hz for  $M_1$  (Fig. 9(a)) to 22.5 Hz for  $M_3$ . This is because the compressing of the isolator dominated the contributions to the value of stiffness, and because the stiffness dominated the response at low frequencies.

The obtained transmissibility values of the five isolators are compared in Fig. 10. This comparison was done for the third level of acceleration and using the third mass  $M_3$ . From model A to model E, the resonance frequency increases and the

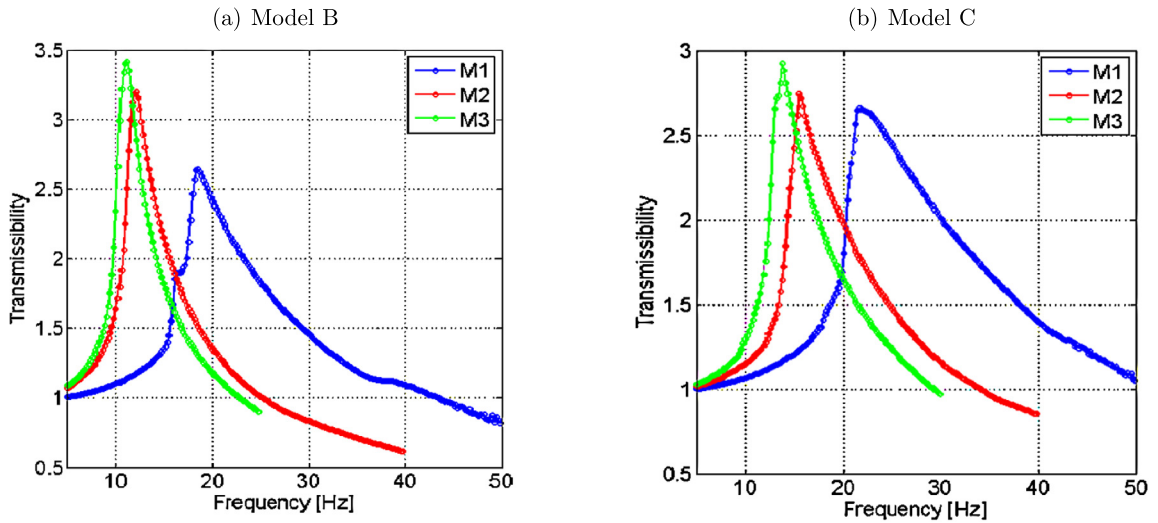


Fig. 9. Sine sweep test; acceleration 2 m/s<sup>2</sup>.

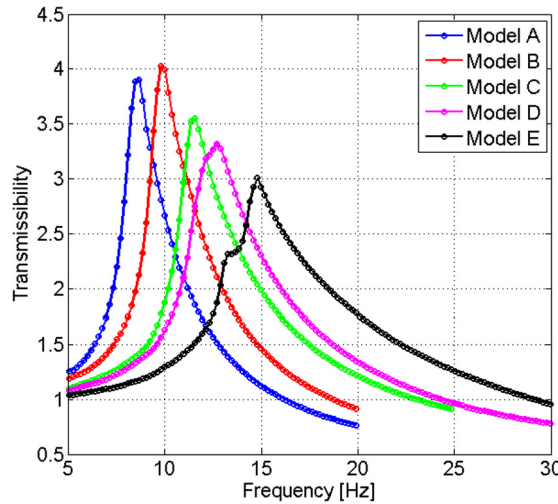


Fig. 10. Sine sweep test; mass 3, acceleration 3 m/s<sup>2</sup>.

amplitude decreases. In addition, the frequency at which the system is isolated (transmissibility less than one), increases also. This means that, the higher the density of the isolator, the larger the isolation frequency bandwidth.

Now, a vibration test was conducted with both increasing and decreasing frequencies. Experiments were performed using isolator model C, under  $M_3$  and for levels of acceleration of 2 m/s<sup>2</sup> and 3 m/s<sup>2</sup>. Graphs of the run-up sweep and of the run-down sweep are shown in Fig. 11(a, b); the down-sweep peak shifts away from the up-sweep peak. Hysteresis and the jump phenomena are observed [29]. These are the characteristic of the softening behaviour of the metal mesh isolator.

#### 4.4. Nonlinear modelling

##### 4.4.1. Application of the method

The transmissibility values measured for three levels of excitation have been analysed with the CONCERTO approach that was established in section 2 and validated in section 3. For the sake of clarity, only the results obtained with  $M_2$  will be presented.

Figs. 12–16 show the variation of stiffness and damping as a function of the displacement. The data shown in these figures have been normalised. The normalisation ratio of stiffness and damping against the amplitude of the vibration displacement is consistent rather than random.

These figures show the stiffness and the damping decreases with an increase in the displacement. As the level of excitation increases, the response displacement increases too, while the values of stiffness and damping decrease. What is

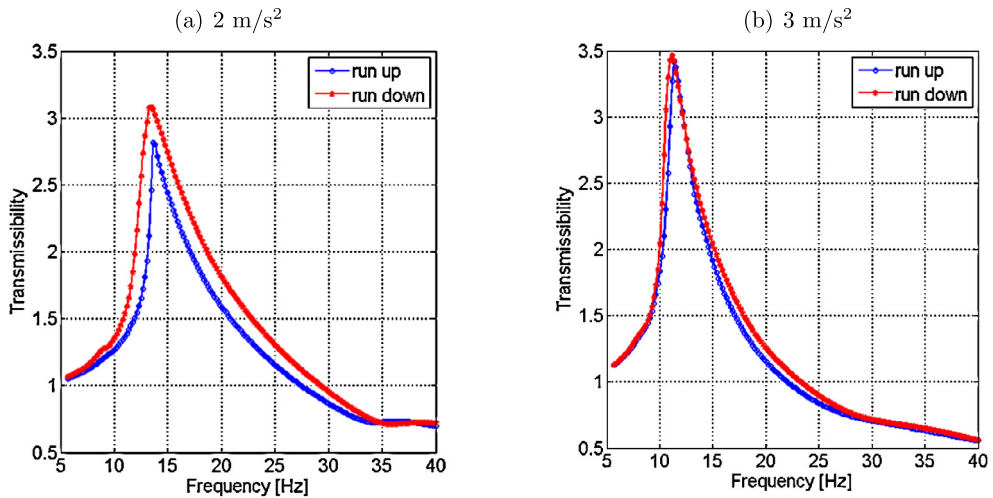


Fig. 11. Sine sweep test; model C, mass 3.

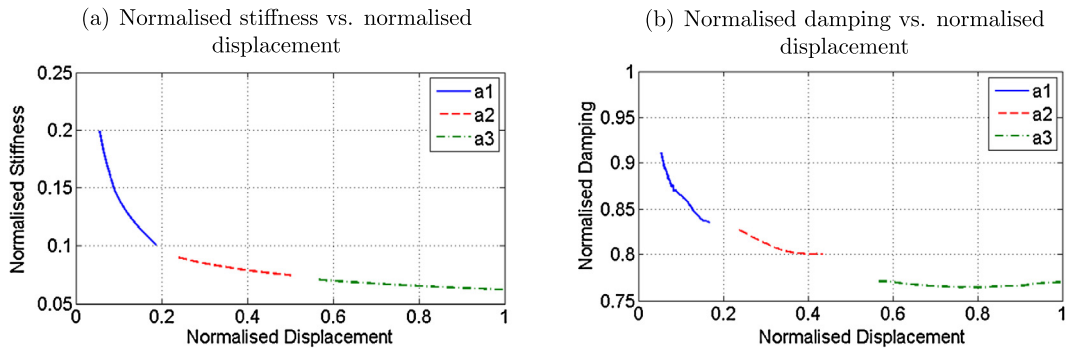


Fig. 12. Extracted stiffness and damping from experimental data; model A, mass 2.

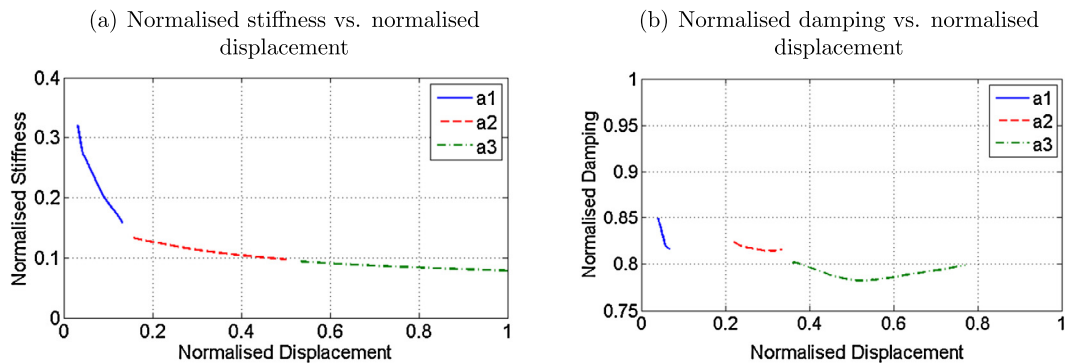


Fig. 13. Extracted stiffness and damping from experimental data; model B, mass 2.

remarkable is that the softening type nonlinearity of the mesh isolator is clearly visible, similar to what was shown in section 4.3.

On the other hand, we notice that, from isolator A to isolator E, stiffness increases. This fact is due to the manufacturing and knit method used for each isolator.

#### 4.4.2. Identification of the nonlinear parameters of the isolator

The MATLAB basic fitting approach is applied to the curves extracted from CONCERTO, shown in Figs. 12–16 to determine the stiffness and damping functions. The functions describing the fitted curve stiffness and damping from the curve fitting are as follows:

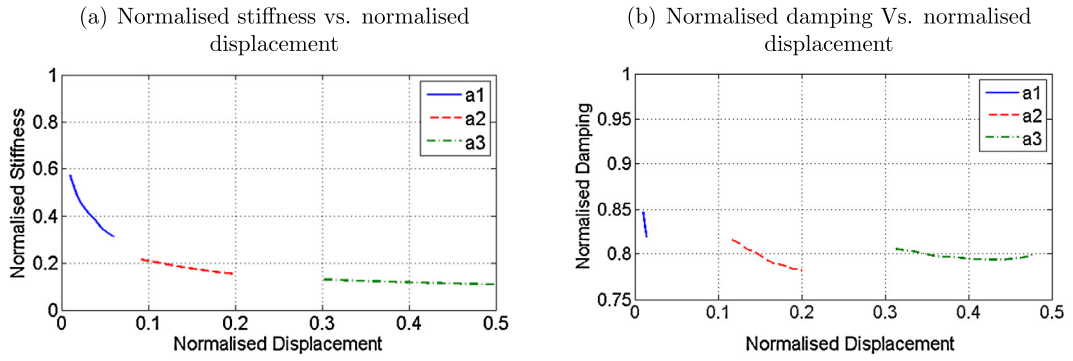


Fig. 14. Extracted stiffness and damping from the experimental data; model C, mass 2.

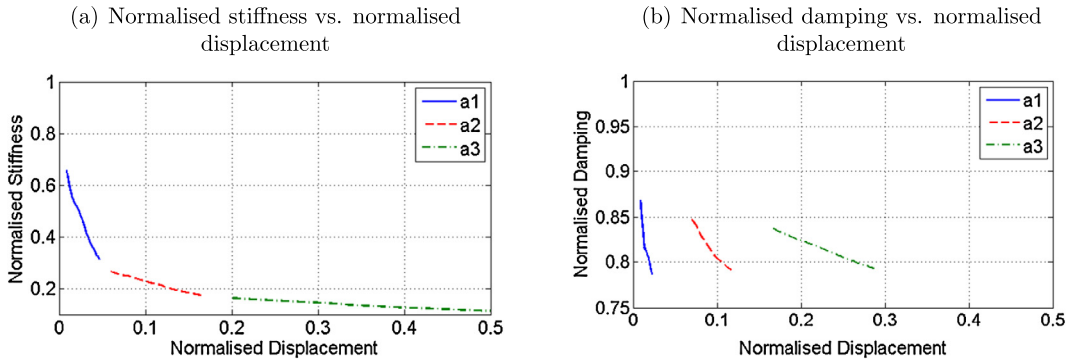


Fig. 15. Extracted stiffness and damping from the experimental data; Model D, Mass 2.

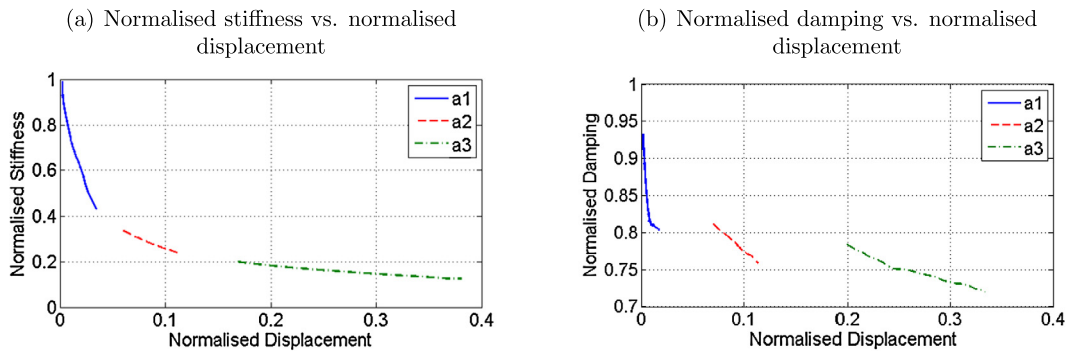


Fig. 16. Extracted stiffness and damping from experimental data; model E, mass 2.

$$K_{\text{fitted}} = \alpha_1 + \alpha_2 Z + \alpha_3 Z^2 \tag{23}$$

$$C_{\text{fitted}} = \mu_1 + \mu_3 Z^2 \tag{24}$$

where  $(\alpha_1, \alpha_2, \alpha_3)$  and  $(\mu_1, \mu_3)$  are the coefficients determined from MATLAB basic fitting.

Combining the equations (23)–(24) and the equivalent stiffness (Eq. (25)) and damping (Eq. (26)) functions proposed by [28], the nonlinear stiffness coefficients  $(k_1, k_2, k_3)$  and the nonlinear damping coefficients  $(c_1, c_3)$  of the isolator can be identified, as shown in Table 3.

$$K_{\text{eq}} = k_1 + \frac{8}{3\pi} k_2 Z + \frac{3}{4} k_3 Z^2 \tag{25}$$

$$C_{\text{eq}} = c_1 + \frac{3}{4} \omega^2 c_3 Z^2 \tag{26}$$

As an example, the measured transmissibility curve of the isolator type A, obtained with  $M_2$  excited by the second acceleration ( $a_2 = 2 \text{ m/s}^2$ ), is plotted as a blue line in Fig. 17. In the same figure, the numerical solution using direct integration using ODE45 is shown for comparison.

**Table 3**

Identified results of stiffness and damping coefficients.

| Coefficients | $k_1$               | $k_2$                | $k_3$               | $c_1$               | $c_3$                           |
|--------------|---------------------|----------------------|---------------------|---------------------|---------------------------------|
| Value        | $3.7417 \cdot 10^4$ | $-1.3135 \cdot 10^7$ | $4.0131 \cdot 10^9$ | $1.3366 \cdot 10^2$ | $1.4544 \cdot 10^4$             |
| Unit         | N/m                 | N/m <sup>2</sup>     | N/m <sup>3</sup>    | Ns/m                | Ns <sup>3</sup> /m <sup>3</sup> |

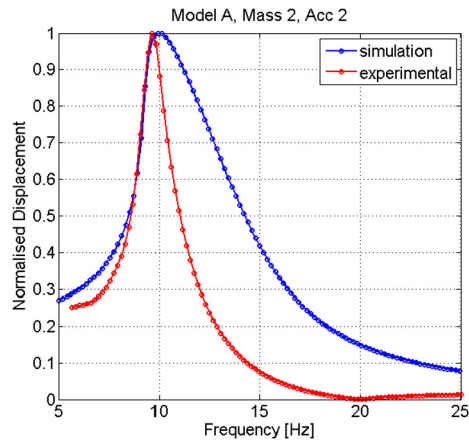
**Fig. 17.** Comparison between the numerical simulation and the measured data; model A, mass 3, acceleration 2 m/s<sup>2</sup>.

Fig. 17 indicates the good agreement between simulations and experiments in the first branch (before the peak). Otherwise, the most important particularity is that the adjacency in the resonant frequency and the amplitude of the resonance are almost close. This proves the validity of the assumption used in the method to identify the dynamic characteristic of the isolator from measured data, as mentioned in [27]. The shift between the curves in the second branch (after peak) is similar to the results, as shown in [27]. The shift might be related to the identified damping coefficients that have been implemented in the model (defined in Eq. (21)). The damping function defined in [30], in which the damping force is a combination of coulombic damping, quadratic damping, and viscous damping, could be implemented in the model to achieve good coherence.

## 5. Conclusion

Nonlinearities in structural dynamics are common in real structures. The identification of nonlinearity parameters from experimental data is an important step to obtain a reliable and precise numerical model that will ensure a better understanding of their dynamical behaviour. This paper reviews the state of the art of the theory of vibration isolation and presents several types of nonlinear isolators. Thus, different methods of identification are presented. One of them is investigated in order to characterise the dynamic behaviour of a SDOF system. This approach consists in realising several steps: firstly, this method is compared with an existent identification method to validate it; then, a practical application to an anti-vibration isolator is presented and the linear and nonlinear parameters are extracted to be used for building a theoretical model that will be used for numerical simulation. The agreement between the simulated and measured results is acceptable. But errors are introduced in the estimation of damping. The cause of these errors has not been fully understood and it can be speculated that this is the jump phenomenon effect. Most importantly, future works will focus on three different aspects: for instance, further exploration will be done to identify the limitations in order to improve the method presented; in addition, these works will investigate the influence of the temperature in the behaviour of the nonlinear isolator; moreover, future research should also consider the identification issues arising from the dynamic driving point stiffness using impact tests.

## References

- [1] Z.M. Ripin, O.L. Ean, Dynamic characterization of engine mount at different orientation using sine swept frequency test, in: Regional Conference on Mechanical and Aerospace Rechnology, Sanur, Bali, 9–10 February 2010, 2010, pp. 1–6.
- [2] P. Polach, M. Hajžman, Design of characteristics of air-pressure-controlled hydraulic shock absorbers in an intercity bus, *Multibody Syst. Dyn.* 19 (1–2) (2008) 73–90.
- [3] R. Ibrahim, Recent advances in nonlinear passive vibration isolators, *J. Sound Vib.* 314 (3) (2008) 371–452.
- [4] C. Yilmaz, N. Kikuchi, Analysis and design of passive band-stop filter-type vibration isolators for low-frequency applications, *J. Sound Vib.* 291 (3) (2006) 1004–1028.
- [5] J. Winterflood, D.G. Blair, B. Slagmolen, High performance vibration isolation using springs in Euler column buckling mode, *Phys. Lett. A* 300 (2) (2002) 122–130.
- [6] N. Du Plooy, P. Heyns, M. Brennan, The development of a tunable vibration absorbing isolator, *Int. J. Mech. Sci.* 47 (7) (2005) 983–997.

- [7] X. Gao, Q. Chen, H. Teng, Modelling and dynamic properties of a novel solid and liquid mixture vibration isolator, *J. Sound Vib.* 331 (16) (2012) 3695–3709.
- [8] M. Yamamoto, Compression spring, Japan, Japanese Patent (1992) 04-370427.
- [9] W.A. Courtney, Preliminary Investigations Into the Mechanical Properties and Potential Applications of a Novel Shock Absorbing Liquid, University of Manchester, UK, 1998.
- [10] W. Courtney, S. Oyadiji, Preliminary investigations into the mechanical properties of a novel shock absorbing elastomeric composite, *J. Mater. Process. Technol.* 119 (1) (2001) 379–386.
- [11] D.L. Platus, Negative-stiffness-mechanism vibration isolation systems, in: San Jose-DL Tentative, International Society for Optics and Photonics, 1992, pp. 44–54.
- [12] A. Carrella, M. Brennan, T. Waters, V. Lopes, Force and displacement transmissibility of a nonlinear isolator with high-static-low-dynamic-stiffness, *Int. J. Mech. Sci.* 55 (1) (2012) 22–29.
- [13] S.-H. Youn, Y.-S. Jang, J.-H. Han, Development of a three-axis hybrid mesh isolator using the pseudoelasticity of a shape memory alloy, *Smart Mater. Struct.* 20 (7) (2011) 075017.
- [14] L. Jezequel, C.-H. Lamarque, Analysis of non-linear dynamical systems by the normal form theory, *J. Sound Vib.* 149 (3) (1991) 429–459.
- [15] R. Lin, Identification of the Dynamic Characteristics of Nonlinear Structures, PhD thesis, University of London, 1990.
- [16] K. Worden, G.R. Tomlinson, Nonlinearity in Structural Dynamics: Detection, Identification and Modelling, CRC Press, Boca Raton, FL, USA, 2000.
- [17] M. Feldman, Non-linear system vibration analysis using Hilbert transform – I. Free vibration analysis method 'freevib', *Mech. Syst. Signal Process.* 8 (2) (1994) 119–127.
- [18] M. Feldman, Non-linear system vibration analysis using Hilbert transform – II. Forced vibration analysis method 'forcevib', *Mech. Syst. Signal Process.* 8 (3) (1994) 309–318.
- [19] G. Kerschen, K. Worden, A.F. Vakakis, J.-C. Golinval, Past, present and future of nonlinear system identification in structural dynamics, *Mech. Syst. Signal Process.* 20 (3) (2006) 505–592.
- [20] S. Masri, T. Caughey, A nonparametric identification technique for nonlinear dynamic problems, *J. Appl. Mech.* 46 (2) (1979) 433–447.
- [21] J. He, D. Ewins, A simple method of interpretation for the modal analysis of nonlinear systems, in: 5th International Modal Analysis Conference, London, England, 1987, pp. 626–634.
- [22] D. Göge, M. Sinapius, U. Füllekrug, M. Link, Detection and description of non-linear phenomena in experimental modal analysis via linearity plots, *Int. J. Non-Linear Mech.* 40 (1) (2005) 27–48.
- [23] H. Rice, Identification of weakly non-linear systems using equivalent linearization, *J. Sound Vib.* 185 (3) (1995) 473–481.
- [24] P. Guo, Damping System Designs Using Nonlinear Frequency Analysis Approach, PhD thesis, University of Sheffield, UK, 2012.
- [25] A. Cappellini, A. Carrella, M. Feldman, Measuring dynamic nonlinearities using the frequency response and the Hilbert transform methods, in: Proceedings of the ISMA2010–USD2010 Conference, Leuven, Belgium, 20–22 September 2010, 2010, pp. 3087–3097.
- [26] A. Carrella, D. Ewins, Identifying and quantifying structural nonlinearities in engineering applications from measured frequency response functions, *Mech. Syst. Signal Process.* 25 (3) (2011) 1011–1027.
- [27] A. Carrella, Nonlinear identifications using transmissibility: dynamic characterisation of anti vibration mounts (AVMs) with standard approach and nonlinear analysis, *Int. J. Mech. Sci.* 63 (1) (2012) 74–85.
- [28] G. Wang, G. Zheng, Vibration of two beams connected by nonlinear isolators: analytical and experimental study, *Nonlinear Dyn.* 62 (3) (2010) 507–519.
- [29] M. Amabili, M. Pellegrini, M. Tommesani, Experiments on large-amplitude vibrations of a circular cylindrical panel, *J. Sound Vib.* 260 (3) (2003) 537–547.
- [30] Z. Hu, G. Zheng, A combined dynamic analysis method for geometrically nonlinear vibration isolators with elastic rings, *Mech. Syst. Signal Process.* 76 (2016) 634–648.